Inorganic Chemistry

pubs.acs.org/IC Article

Strong Coupling and Slow Relaxation of the Magnetization for an Air-Stable [Co₄] Square with Both Tetrazine Radicals and Azido Bridges

Zhilin Guo, Yi-Fei Deng,* Zoe Pikramenou, Kim R. Dunbar,* and Yuan-Zhu Zhang*



Cite This: Inorg. Chem. 2021, 60, 3651–3656



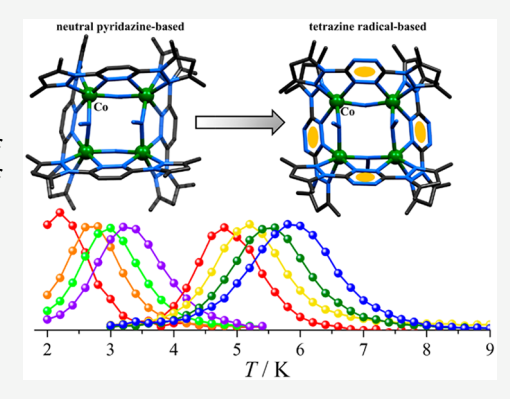
ACCESS

III Metrics & More

Article Recommendations

s) Supporting Information

ABSTRACT: Introducing both tetrazine radical and azido bridges afforded two air-stable square complexes $[M^{II}_{4}(bpztz^{\bullet-})_{4}(N_{3})_{4}]$ ($M^{II} = Zn^{2+}$, 1; Co^{2+} , 2; bpztz = 3,6-bis(3,5-dimethylpyrazolyl)-1,2,4,5-tetrazine), where the metal ions are cobridged by $\mu_{1,1}$ -azido bridges and tetrazine radicals. Magnetic studies revealed strong antiferromagnetic metal—radical interaction with a coupling constant of -64.7 cm⁻¹ in the 2*J* formalism in 2. Remarkably, 2 exhibits slow relaxation of magnetization with an effective barrier for spin reverse of 96 K at zero applied field.



■ INTRODUCTION

Coordination-driven self-assembly¹ of supramolecular architectures continues to produce fascinating results in many interdisciplinary fields with various fundamental applications² including sensors, optics, spintronics, and catalysis. Elegant and intricate structures such as metallacycles, molecular knots, metal—organic polyhedra, metallocages, and interlocked molecules have been reported because of the structural versatility of the metal ions and the directionality of the metal—ligand interactions based on the coordination algorithm.³ A key underpinning of research on this topic is the design of specific organic linkers that are coded to produce a desired topology. Of specific interest to the present work is the use of organic radical linkers in supramolecular architectures that exhibit strong direct magnetic couplings.⁴

The literature is replete with examples of compounds featuring metal spins coupled through closed-shell bridging ligands via an indirect superexchange mechanism, but many of these magnetic interactions are relatively weak especially when the bridging ligand spans a large distance. Although the chemistry is more challenging, the use of free radical bridges⁵ is capable of propagating efficient spin exchange beyond the limit of distance and gives rise to much stronger magnetic interactions due to the direct overlap of orbitals that bears the unpaired electrons. The growing body of research in this area has demonstrated that higher blocking temperatures for single-molecule magnets (SMMs) are achieved with paramagnetic bridges.⁶ A remarkable recent example is a radical bridged dinuclear Co(II) compound that exhibits significantly higher relaxation times and hysteresis up to 15 K, among the

very best properties reported for transition-metal-based SMMs. $^{\rm 6c}$

The most common motif for supramolecular metallacycles is the molecular square which is due to the ease of satisfying the requirement for 90° angles between the metal corners with the use of linear organic linkers.³ Specifically, 3,6-substituted pyridazine and tetrazine derivatives have been used for the formation of various polygonal topologies including triangles, squares, and pentagons mostly through the trans-bridging mode. Such preprogrammed topologies with tetrazine radical ligands haven been incorporated into coordination complexes including recent work from Dunbar and Murugesu groups, who demonstrated that much stronger ferromagnetic or antiferromagnetic coupling up to $J \approx \pm 100 \text{ cm}^{-1}$ (in 2J formalism) between tetrazine radicals and paramagnetic metal ions can be realized; however, less SMM behavior was observed.⁸ Given that the contribution to the spin reversal barrier in most transition-metal complexes is dominated by axial zero-field splitting (D) and the magnetic coupling (J) these parameters are important to control. It is well-known that the end-on (EO, $\mu_{1,1}$) azido bridge would engender appreciable and predictable ferromagnetic coupling, and we

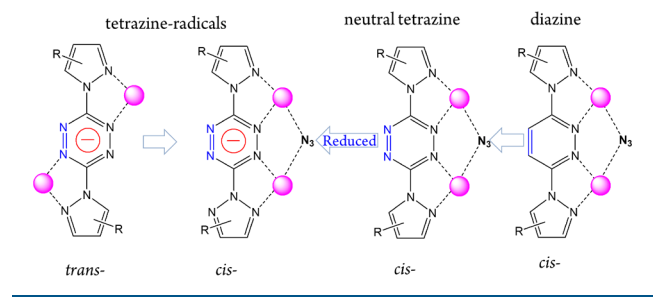
Received: October 26, 2020 Published: March 3, 2021





recently incorporated azide ions as secondary bridges and constructed two [Co₄] square complexes, {[(L)₄Co^{II}₄($\mu_{1,1}$ -N₃)₄][BPh₄]₄}·sol (2a, L = 3,6-bis(3,5-dimethyl-1H-pyrazol-1-yl)pyridazine (pzdz); 2b, L = 3,6-di(pyridin-2-yl)pyridazine (pydz)), in which the neutral pyridazine derivatives adopt *cis*-bridging modes as dictated by the EO–azido bridge (Scheme 1). The ferromagnetic coupling constant was found to be approximately +4 cm⁻¹, and both compounds exhibit typical field-induced slow relaxation in magnetization. ¹⁰

Scheme 1. Coordination Modes of Tetrazines/Diazines



With this prior work as a backdrop as well as the above considerations, the related tetrazine derivative of bpztz anion radical formation was thus explored in the assembly of metal complexes within the selected topology bearing azide bridging ligand to further improve the magnetic communication. Herein we report the synthesis, structures and magnetic studies of the air-stable azido-bpztz cobridged molecular squares $[M^{II}_{4}(bpztz^{\bullet-})_{4}(N_{3})_{4}]$ $(M^{II}=Zn^{2+},~1;~Co^{2+},~2)$. Crystallographic and magnetic studies revealed a rare cis-tetrazine radical bridged [M₄] square structure with magnetic coupling for 2 being significantly enhanced for the radical versus the diamagnetic bridging ligand. As a result, high-performance magnetic relaxation behavior with an effective energy barrier of 96 K of 2 at zero dc field and clear magnetic hysteresis loops below 5 K were observed, which is the first example of a cistetrazine radical bridged [Co₄] square and among the highest relaxation barriers for reported polynuclear Co(II) compounds.

■ RESULTS AND DISCUSSION

Syntheses and Crystallographic Studies. Treatment of $[Zn(H_2O)_6][ClO_4]_2$ or $[Co(H_2O)_6][ClO_4]_2$ with bpztz ligand in a 1:1 ratio with slight excess of sodium azide and L-ascorbic acid in an inert atmosphere yielded compounds 1 and 2. Single-crystal X-ray diffraction (SCXRD) studies revealed that 1 and 2 crystallize in the tetragonal space group I4₁/acd (Table S1). Select bond distances and angles are listed in Table S2. Bond valence sum (BVS) calculations (Table S3) indicate the presence of 2+ oxidation state of Co and Zn which, considering the overall charge balance, means that all bpztz ligands have been reduced to radicals. This was further confirmed by room-temperature EPR data of 1 in solid state which gave a Lande factor $g_{rad} = 2.003$ (Figure S1). Powder Xray diffraction patters of 1 and 2 under ambient conditions matched well with the SCXRD simulation (Figure S2), indicating high purity and air stability for the compound.

As shown in Figure 1, the neighboring metal ions reside at corners and are linked by one bpztz ligand in a *cis* mode and one $\mu_{1,1}$ -azido bridge to form a neutral molecular square [M₄]. There are two crystallographically independent metal ions (M1 and M2) in the asymmetric unit. Each M^{II} ion adopts a

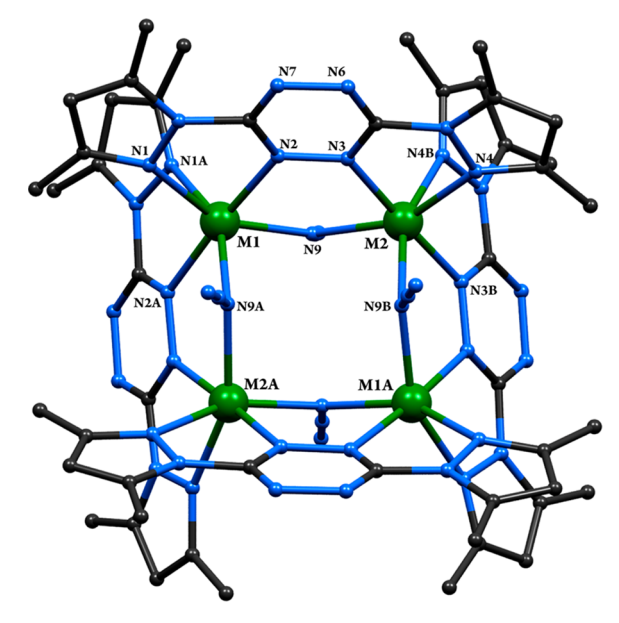


Figure 1. A ball-and-stick structure of 1 ($M = Zn^{2+}$) and 2 ($M = Co^{2+}$) with a numbering scheme. Hydrogen atoms were omitted for the sake of clarity.

distorted octahedral coordination geometry formed by four N atoms from two different bpztz ligands and two N atoms from azido ligands. The M-N bond distances and the cis N-M-N angles are in the ranges 2.082-2.231 Å and 71.23°-111.08° for 1 and 2.052-2.185 Å and 74.51°-111.92° for 2. The Co-N bond distances in 2 are consistent with those for a high-spin Co(II) ion. The bridging M-N_{azido}-M angle is 117.63° for 1 and 117.89° for 2. Significant elongation of the N-N intratetrazine bond distances of 1.378 Å (N2-N3) and 1.400 Å (N6–N7) in 1 and 1.377 Å (N2–N3) and 1.397 Å (N6–N7) in 2 compared with the neutral tetrazine ligand ($\sim 1.32 \text{ Å}$) strongly supports the formation of tetrazine radical in 1 and 2.8c,11 It should be mentioned that the dihedral angles between the pyrazolyl and tetrazine rings of the bpztz ligand in 2 are 3.32° and 10.21°, indicating increased coplanarity compared to the previously reported diamagnetic analogues (4.19°- 26.06°). Moreover, the chelating N_{pz} -M- N_{tz} (N1-Co1-N2 and N3-Co2-N4) angles of 74.51° and 72.41° in 2 are significantly smaller than those for the related $[Co_4]$ complexes in a trans binding mode. 8f The [Co₄] core is nearly planar with adjacent Co···Co distances of 3.606 Å and vertex Co-Co-Co angles of 92.83° and 87.17° for 2 with similar parameters of 3.617 Å, 92.38° , and 87.62° for 1. The shortest intermolecular M...M separation is 9.98 and 10.29 Å for 1 and 2, respectively. It is worth noting that extensive short contacts were found throughout the 3D packing arrangement involving weak H_{pz} ... N_{azide} hydrogen bonds (1, 3.042 Å; 2, 3.142 Å), noncovalent $C-H\cdots\pi$ interactions (1, 2.455–3.217 Å; 2, 2.418–3.232 Å), and edge-to-edge (1, 4.107 Å; 2, 4.072 Å) $\pi \cdots \pi$ interactions (Figures S3 and S4). Such supramolecular interactions give rise to appreciable intermolecular magnetic interactions which accounts for the long-range antiferromagnetic ordering for this large spin system (vide infra).

UV-Vis Spectroscopy Studies. UV-vis spectroscopy is also performed to study the tetrazine radical formation. In solution, the neutral bpztz ligand shows a strong $\pi-\pi^*$ transition at 298 nm and less intense $n-\pi^*$ transition bands in the visible region (Figure 2). To 1 and 2, the $\pi-\pi^*$

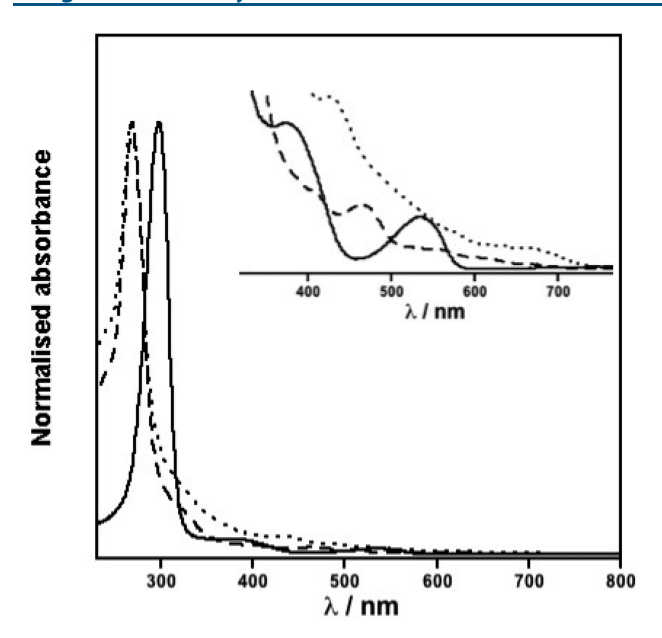


Figure 2. UV-vis spectra of bpztz ligand (solid line), 1 (dashed line), and 2 (dotted line) in CH₂Cl₂ solution.

transition bands are blue-shifted to 280 nm due to decreased conjugation. The absorption bands at visible region show a clear red-shift which is the influence of $n-\pi^*$ contributions upon coordination. This is consistent with the previously reported N-heterocylic radicals, ¹³ which clearly supports the tetrazine radicals in 1 and 2. At solid state (Figure S5), the band at 530 nm of the spectrum can be possibly attributed to excimer formation. The bands of 1 and 2 at the solid state can be also attributed to packing or extensive electronic communication between ligands which alters the HOMO–LUMO of the $n-p^*$ transition.

Cyclic Voltammetry Studies. The electrochemical property of **2** studied by cyclic voltammetry method in dichloromethane revealed four consecutive and reversible redox potentials at $E_{1/2} = +0.31$, +0.47, +0.63, and +0.79 V (vs Ag/AgCl), which were assigned to the four one-electron oxidation processes of $[\text{Co}^{\text{III}}_{1}\text{Co}^{\text{II}}_{3}]^{+}$, $[\text{Co}^{\text{III}}_{2}\text{Co}^{\text{II}}_{2}]^{2+}$, $[\text{Co}^{\text{III}}_{3}\text{Co}^{\text{II}}_{1}]^{3+}$, and $[\text{Co}^{\text{III}}_{4}]^{4+}$ states, respectively. In addition, the reversible one-electron reduction at $E_{1/2} = -1.3$ V is most likely attributed to bpztz radical reduction (Figure 3). Given that ΔE (the redox potential difference) is the same (0.16 V) for the four redox waves, the calculated comproportionation constants (K_c) based on $K_c = \exp(F\Delta E/RT)$ were found to be 5.07 \times 10², indicating the intermediated stability of mixed valence states.

Magnetic Studies. Variable-temperature magnetic susceptibility data for 1 and 2 were collected with applied direct current (dc) fields of 0.1 and 1 kOe (Figure 4 and Figure S6). The χT value at 300 K of 1.46 cm³ mol⁻¹ K for 1 is consistent with four noninteracting bpztz⁵⁻ radicals ($S_{\rm rad}=1/2, g=2.003$). Upon cooling, the χT value remains essentially constant down to 50 K and then decreases to 0.122 cm³ K mol⁻¹ at 2 K, indicating antiferromagnetic (AF) interactions between the radicals. In the case of 2, the χT value of 13.67 cm³ K mol⁻¹ at 300 K is significantly higher than the theoretically calculated for four isolated high-spin Co¹l ions (1.875 cm³ K mol⁻¹ each) and four uncoupled bpztz⁵⁻ radicals, indicating the significant orbital contribution. ¹⁴ Upon cooling, the χT value increases continuously to a

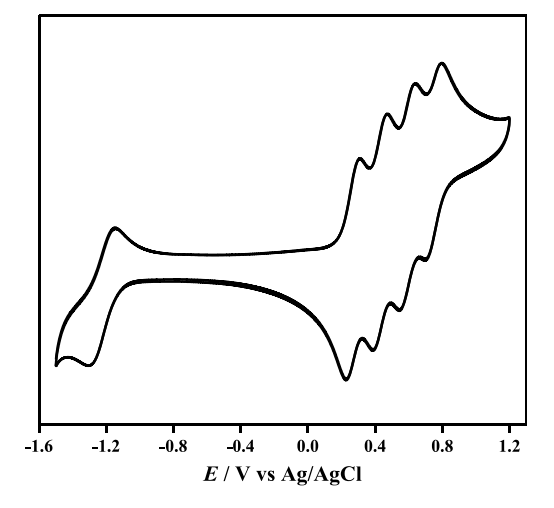


Figure 3. Cyclic voltammetry spectrum of 2 in CH_2Cl_2 solution (in 0.1 M $[n\text{-Bu}_4N][PF_6]$ supporting electrolyte) with a Pt working electrode at a scan rate of 0.1 V/s at room temperature.

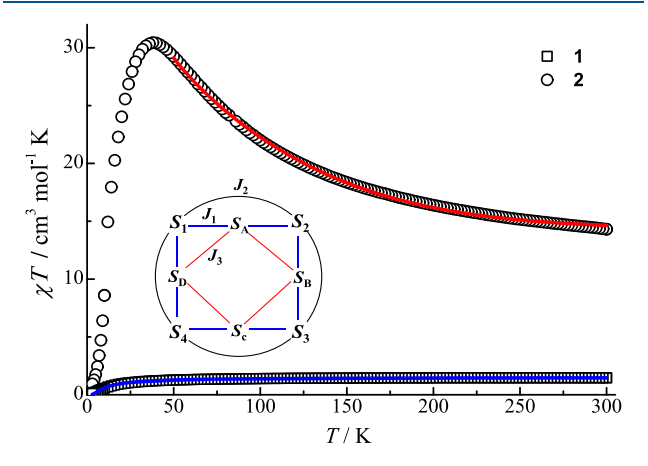


Figure 4. Variable-temperature magnetic susceptibility data for 1 (\square) and 2 (\bigcirc) under an applied dc field of 1 kOe. Solid lines represent the fittings based in eqs 1 and 2. The inset shows the magnetic exchange pathways in 2.

maximum of 29.16 cm³ mol⁻¹ K at 37 K and then decreases to 0.64 cm³ K mol⁻¹ at 2 K, likely due to the presence of intermolecular AF interactions, magnetic anisotropy, and/or blocking dynamics.

To probe the magnetic coupling between the spin carriers, the magnetic susceptibility data for 1 (2-300 K) and 2 (50-300 K) were fitted by using the PHI program¹⁵ based on the following spin Hamiltonian (eq 1 for 1 and eq 2 for 2):

$$\hat{H} = -2J_{3}(\hat{S}_{A}\hat{S}_{B} + \hat{S}_{B}\hat{S}_{C} + \hat{S}_{C}\hat{S}_{D} + \hat{S}_{D}\hat{S}_{A}) + (\sum_{i=A}^{D} g_{rad}\mu_{B}\hat{S}_{i}H)$$

$$\hat{H} = -2J_{1}(\hat{S}_{1}\hat{S}_{A} + \hat{S}_{A}\hat{S}_{2} + \hat{S}_{2}\hat{S}_{B} + \hat{S}_{B}\hat{S}_{3} + \hat{S}_{3}\hat{S}_{C} + \hat{S}_{C}\hat{S}_{4}$$
(1)

$$+ \hat{S}_{4}\hat{S}_{D} + \hat{S}_{D}\hat{S}_{1}) + (\sum_{i=A}^{D} g_{\text{rad}} \mu_{B} \hat{S}_{i} H) + (\sum_{i=1}^{4} g_{\text{Co}} \mu_{B} \hat{S}_{i} H)$$

$$- 2J_{2}(\hat{S}_{1}\hat{S}_{2} + \hat{S}_{2}\hat{S}_{3} + \hat{S}_{3}\hat{S}_{4} + \hat{S}_{4}\hat{S}_{1})$$

$$- 2J_{3}(\hat{S}_{A}\hat{S}_{B} + \hat{S}_{B}\hat{S}_{C} + \hat{S}_{C}\hat{S}_{D} + \hat{S}_{D}\hat{S}_{A})$$
(2)

where S_1 to $S_4 = S_{Co} = 3/2$, S_A to $S_D = S_{rad} = 1/2$, μ_B is the Bohr magneton, H is the magnetic field vector, and g_{Co} and g_{rad} (2.003 as determined by EPR studies) are the Lande factors for the Co(II) ion and bpztz $^{\bullet-}$ radical, respectively; I_1 to I_3 correspond to the magnetic couplings for Co--radical, Co--Co, and the neighboring radicals, respectively. It should be mentioned that no acceptable fitting of χT vs T plots was achieved over the 2-300 K temperature range by using an anisotropic spin model, possibly due to the low-temperature complexity including the metamagnetism, antiferromagnetic ordering, and relaxation dynamics. In addition, the incorporation of more anisotropic parameters in this advanced model would lead to the overparametrization. On the basis that the high-temperature magnetic susceptibility should be dominated by the strong exchange couplings mediated by bptz*- radicals, the χT vs T plots at above 50 K were thus fitted with an isotropic spin model. Moreover, given that the [Zn₄] analogue (1) can be unambiguously characterized over the entire temperature, the coupling constant between the neighboring bpztz* radicals was thus restrained as the same across the two data sets of 1 and 2 to avoid the overparametrization. With the addition of the intermolecular couplings (zj') based on the mean-field approximation, ¹⁶ the best fitting gave $J_3 = -4.7$ cm⁻¹ and zj' = -0.2 cm⁻¹ for **1**. For **2**, zj' can be neglected in the high-temperature range, and J_3 was fixed to -4.7 cm⁻¹ in the fitting process to reduce the parameter space. The best set of parameters are $J_1 = -64.7$ cm⁻¹, $J_2 = +4.9$ cm⁻¹, and $g_{Co} =$ 2.81. It should be noted that attempts to fit the susceptibility data of 2 with a free J_3 parameter did not improve the quality significantly and gave similar results. The obtained $J_{\text{Co-rad}}$ value is similar to that observed for bptz*- radical bridged [CoII3] (-67.5 cm^{-1}) and $[\text{Co}_{4}^{\text{II}}]$ (-66.8 cm^{-1}) complexes¹⁰ and confirms the strong AF coupling between the Co(II) metal centers and bpztz*- radicals.

The isothermal field-dependent magnetization of 2 measured at 2 K exhibits a pronounced sigmoidal behavior with an initial slow increase (Figure S7), corresponding to an AF ordered state, and then a sharp transition to a superparamagnetic state, reaching an unsaturated value of 11.4 N β at 70 kOe, typical for a metamagnet with the critical field of 32.5 kOe, extracted from the peak in its dM/dH curve (Figure S8). Such behavior is indicative of metamagnetic behavior which comes from the weak intersquare couplings. The lack of saturation reveals the presence of magnetic anisotropy. Further studies revealed that the critical fields decrease at higher temperatures, and the S-shape disappears at temperatures above 12 K. The metamagnetic behavior is further supported by the field-cooled (FC) magnetization measurements under fields of 1-35 kOe (Figure S9). Moreover, specific heat measurements reveal a λ -shaped peak at \sim 11.5 K under zero field and disappeared under an applied dc field of 30 kOe, which unambiguously corroborated the antiferromagnetic ordering and metamagnetic behavior of 2 (Figure S10).

Remarkably, stepwise magnetic hysteresis loops at a field sweep rate of 20 Oe/s were observed below 4.0 K (Figure 5). At 2 K, a wide stepwise hysteresis loop with a coercive field of 9 kOe and a remnant magnetization ($M_{\rm R}$) of 2.2 N β was observed. The loops exhibit narrowing at higher temperatures and disappear at temperatures above 4 K. In terms of the ZFC-FC experiments, under an applied dc field of 50 Oe, the ZFC-FC splitting at about 12 K is much higher than the blocking temperature where the hysteresis closes (Figure S11a), which may be caused by the coexistence of AF ordering and magnetic

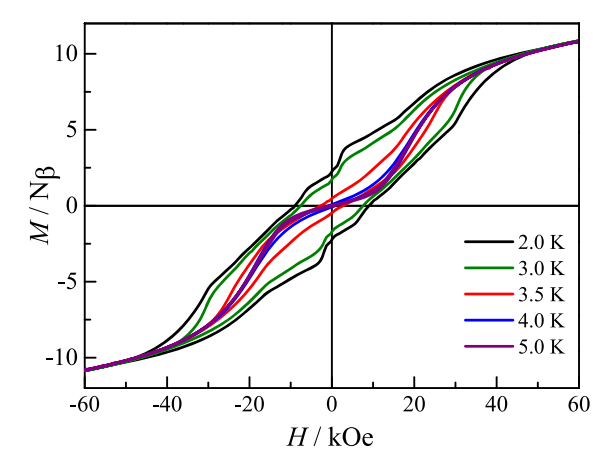


Figure 5. Hysteresis loops of **2** measured at 2–5 K with a field sweep rate of 20 Oe/s. Solid lines are guides for the eye.

relaxation. To better address this, the ZFC-FC plots were further measured under an applied dc field of 30 kOe where the AF ordering is overcome (Figure S11b). As a result, the observed divergence for the ZFC-FC plots at about 4.5 K is in well agreement with the blocking temperature extracted from the hysteresis measurements, indicating that the ZFC-FC splitting is attributed to the blocking dynamics rather than the long-range magnetic ordering.

To investigate the relaxation dynamics of **2**, ac susceptibility data were collected under zero and 30 kOe applied dc fields. The in-phase (χ') signals under a zero dc field exhibit frequency-independent signals maximum at 13 K with the out-of-phase (χ'') component remaining zero around this temperature (Figure 6, left). This is not unexpected for

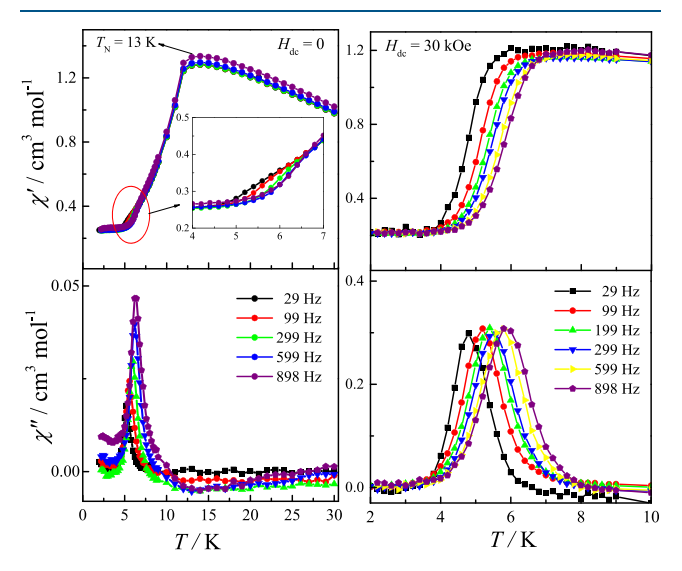


Figure 6. Temperature dependence of the in-phase (χ') and out-of-phase (χ'') ac susceptibility data for **2** at zero (left) and 30 kOe (right) dc fields. Solid lines are guides for the eye.

antiferromagnets and agrees well with the dc results. Interestingly, strong frequency-dependent behavior in the temperature range 4–10 K was observed, although the signals are weak. Under an applied dc field of 30 kOe (above the critical field) to overcome the intercluster AF interactions, both the in-phase and out-of-phase ac susceptibilities exhibit obvious frequency dependence, with the χ'' maximum shifting

from 4.8 K at 29 Hz to 5.9 K at 898 Hz (Figure 6, right). The intensities of the out-of-phase signals increase 10 times. The Mydosh parameter $\varphi = (\Delta T_p/T_p)/(\Delta \log f)$ was estimated to be 0.13, which is larger than a canonical spin glass and closer to a normal value for superparamagnetic behavior. 18 The relaxation time (τ) derived from the χ'' peaks (Table S4) follows the Arrhenius law $\tau = \tau_0 \exp(U_{\text{eff}}/k_{\text{B}}T)$. The obtained effective energy barriers of 96 K ($\tau_0 = 5.2 \times 10^{-11}$ s; zero field) and 83 K ($\tau_0 = 1.7 \times 10^{-10}$ s; 30 kOe dc field) are among the largest reported for polynuclear d-block compounds (Figures S12 and S13). The coexistence of long-range magnetic ordering and slow magnetic relaxation is not unexpected for an anisotropic system.²¹ It should be noted that the relaxation time obtained from ac susceptibility measurements seems much lower than those account for the pronounced ZFC-FC and hysteresis curves. Based on the 3D supramolecular structure and AF ordering dictated by extensive short contacts between the [Co₄] squares, such abnormality is reminiscent of some high-dimensional magnetic systems²² wherein much lower pre-exponential factor and relaxation time are observed due to the variable system size, intermolecular interactions, and/or random defects.

CONCLUSIONS

In summary, two new azido-bridged square complexes with *cis*-bpztz radical bridges are reported. Magnetic studies revealed the introduction of tetrazine radicals into a $[{\rm Co^{II}}_4]$ square system is an effective strategy for engendering direct and strong magnetic interactions between metal spin centers and the radicals. The slow magnetic relaxation behavior of **2** is significantly enhanced compared to the neutral pyridazine-bridged analogues, demonstrating the potential of topological control coupled with magnetic properties of radical bridges. Future work is being directed at synthesizing combinations of various paramagnetic 3d transition metals and tetrazine type ligands in the context of these studies.

ASSOCIATED CONTENT

Supporting Information

The Supporting Information is available free of charge at https://pubs.acs.org/doi/10.1021/acs.inorgchem.0c03158.

Experimental details, crystallographic data, crystal structures, and magnetic measurements (PDF)

Accession Codes

CCDC 1958192–1958193 contain the supplementary crystallographic data for this paper. These data can be obtained free of charge via www.ccdc.cam.ac.uk/data_request/cif, or by emailing data_request@ccdc.cam.ac.uk, or by contacting The Cambridge Crystallographic Data Centre, 12 Union Road, Cambridge CB2 1EZ, UK; fax: +44 1223 336033.

AUTHOR INFORMATION

Corresponding Authors

Yi-Fei Deng — Department of Chemistry, Southern University of Science and Technology, Shenzhen 518055, China; Email: dengyf@sustech.edu.cn

Kim R. Dunbar — Department of Chemistry, Texas A&M University, College Station, Texas 77842, United States; Email: dunbar@chem.tamu.edu

Yuan-Zhu Zhang — Department of Chemistry, Southern University of Science and Technology, Shenzhen 518055, China; orcid.org/0000-0002-1676-2427; Email: zhangyz@sustech.edu.cn

Authors

Zhilin Guo — Department of Chemistry, Southern University of Science and Technology, Shenzhen 518055, China; School of Chemistry, The University of Birmingham, Edgbaston B15 2TT, United Kingdom; ⊙ orcid.org/0000-0001-8813-182X Zoe Pikramenou — School of Chemistry, The University of Birmingham, Edgbaston B15 2TT, United Kingdom; ⊙ orcid.org/0000-0002-6001-1380

Complete contact information is available at: https://pubs.acs.org/10.1021/acs.inorgchem.0c03158

Notes

The authors declare no competing financial interest.

ACKNOWLEDGMENTS

This work was supported by the National Natural Science Foundation of China (No. 21671095 and 21901108), Southern University of Science and Technology, and University of Birmingham. K.R.D. thanks the National Science Foundation (CHE-1808779) and the Welch Foundation (A-1449) for financial support.

REFERENCES

- (1) (a) Fujita, M.; Tominaga, M.; Hori, A.; Therrien, B. Coordination Assemblies from a Pd(II)-Cornered Square Complex. *Acc. Chem. Res.* **2005**, *38*, 369–378. (b) Chakrabarty, R.; Mukherjee, P. S.; Stang, P. J. Supramolecular Coordination: Self-Assembly of Finite Two- and Three-Dimensional Ensembles. *Chem. Rev.* **2011**, *111*, 6810–6918.
- (2) (a) Pluth, M. D.; Bergman, R. G.; Raymond, K. N. Proton-Mediated Chemistry and Catalysis in a Self-Assembled Supramolecular Host. *Acc. Chem. Res.* **2009**, 42, 1650–1659. (b) McConnell, A. J.; Wood, C. S.; Neelakandan, P. P.; Nitschke, J. R. Stimuli-Responsive Metal—Ligand Assemblies. *Chem. Rev.* **2015**, 115, 7729–7793. (c) Sepehrpour, H.; Fu, W.; Sun, Y.; Stang, P. J. Biomedically Relevant Self-Assembled Metallacycles and Metallacages. *J. Am. Chem. Soc.* **2019**, 141, 14005–14020.
- (3) (a) Ruben, M.; Rojo, J.; Romero-Salguero, F. J.; Uppadine, L. H.; Lehn, J.-M. Grid-Type Metal Ion Architectures: Functional Metallosupramolecular Arrays. *Angew. Chem., Int. Ed.* **2004**, 43, 3644–3662. (b) Dawe, L. N.; Shuvaev, K. V.; Thompson, L. K. Polytopic ligand directed self-assembly—polymetallic [n × n] grids versus non-grid oligomers. *Chem. Soc. Rev.* **2009**, 38, 2334–2359. (c) Roberts, D. A.; Pilgrim, B. S.; Nitschke, J. R. Covalent post-assembly modification in metallosupramolecular chemistry. *Chem. Soc. Rev.* **2018**, 47, 626–644.
- (4) (a) Darago, L. E.; Aubrey, M. L.; Yu, C. J.; Gonzalez, M. I.; Long, J. R. Electronic Conductivity, Ferrimagnetic Ordering, and Reductive Insertion Mediated by Organic Mixed-Valence in a Ferric Semiquinoid Metal—Organic Framework. J. Am. Chem. Soc. 2015, 137, 15703—15711. (b) Qu, L.; Iguchi, H.; Takaishi, S.; Habib, F.; Leong, C. F.; D'Alessandro, D. M.; Yoshida, T.; Abe, H.; Nishibori, E.; Yamashita, M. Porous Molecular Conductor: Electrochemical Fabrication of Through-Space Conduction Pathways among Linear Coordination Polymers. J. Am. Chem. Soc. 2019, 141, 6802—6806. (c) Thorarinsdottir, A. E.; Harris, T. D. Metal—Organic Framework Magnets. Chem. Rev. 2020, 120, 8716—8789.
- (5) (a) Kaizaki, S. Coordination effects of nitroxide radicals in transition metal and lanthanide complexes. *Coord. Chem. Rev.* **2006**, 250, 1804–1818. (b) Malrieu, J. P.; Caballol, R.; Calzado, C. J.; de Graaf, C.; Guihéry, N. Magnetic Interactions in Molecules and Highly Correlated Materials: Physical Content, Analytical Derivation, and

Rigorous Extraction of Magnetic Hamiltonians. *Chem. Rev.* **2014**, *114*, 429–492.

- (6) (a) Rinehart, J. D.; Fang, M.; Evans, W. J.; Long, J. R. A N23–Radical-Bridged Terbium Complex Exhibiting Magnetic Hysteresis at 14 K. J. Am. Chem. Soc. 2011, 133, 14236–14239. (b) Demir, S.; Jeon, I.-R.; Long, J. R.; Harris, T. D. Radical Ligand-Containing Single-Molecule Magnets. Coord. Chem. Rev. 2015, 289–290, 149–176. (c) Albold, U.; Bamberger, H.; Hallmen, P. P.; van Slageren, J.; Sarkar, B. Strong Exchange Couplings Drastically Slow Down Magnetization Relaxation in an Air-Stable Cobalt(II)-Radical Single-Molecule Magnet (SMM). Angew. Chem., Int. Ed. 2019, 58, 9802–9806.
- (7) (a) Gao, H.; Zhang, Z.-H.; Jiang, P.; Li, X.-R. Synthesis, Crystal Structures and Properties of the Novel Mononuclear Copper(II) and Tetranuclear Cobalt(II) Complexes with 3,6-bis-(3,5-dimethylpyrazolyl)-pyridazine. Transition Met. Chem. 2006, 31, 1088-1092. (b) Schottel, B. L.; Chifotides, H. T.; Shatruk, M.; Chouai, A.; Pérez, L. M.; Bacsa, J.; Dunbar, K. R. Anion $-\pi$ Interactions as Controlling Elements in Self-Assembly Reactions of Ag(I) Complexes with π -Acidic Aromatic Rings. J. Am. Chem. Soc. 2006, 128, 5895-5912. (c) Chifotides, H. T.; Dunbar, K. R. Anion- π Interactions in Supramolecular Architectures. Acc. Chem. Res. 2013, 46, 894-906. (d) Chifotides, H. T.; Giles, I. D.; Dunbar, K. R. Supramolecular Architectures with π -Acidic 3,6-Bis(2-pyridyl)-1,2,4,5-tetrazine Cavities: Role of Anion $-\pi$ Interactions in the Remarkable Stability of Fe(II) Metallacycles in Solution. J. Am. Chem. Soc. 2013, 135, 3039-3055. (e) Bodman, S. E.; Crowther, A. C.; Geraghty, P. B.; Fitchett, C. M. Structural control: can $[2 \times 2]$ silver grids be formed from 4,5disubstituted 3,6-di(2-pyridyl) pyridazines? CrystEngComm 2015, 17, 81-89. (f) Dolinar, B. S.; Alexandropoulos, D. I.; Vignesh, K. R.; James, T. A.; Dunbar, K. R. Lanthanide Triangles Supported by Radical Bridging Ligands. J. Am. Chem. Soc. 2018, 140, 908-911. (g) Li, B.; Wang, X.-N.; Kirchon, A.; Qin, J.-S.; Pang, J.-D.; Zhuang, G.-L.; Zhou, H.-C. Sophisticated Construction of Electronically Labile Materials: A Neutral, Radical-Rich, Cobalt Valence Tautomeric Triangle. J. Am. Chem. Soc. 2018, 140, 14581-14585. (h) Marino, N.; Bruno, R.; Bentama, A.; Pascual-Alvarez, A.; Lloret, F.; Julve, M.; De Munno, G. Magneto-structural correlations in Ni(ii) [2 × 2] metallogrids featuring a variable number of μ -aquo or μ -hydroxo extra bridges. CrystEngComm 2019, 21, 917-924.
- (8) (a) Ruben, M.; Lehn, J.-M.; Müller, P. Addressing metal centres in supramolecular assemblies. Chem. Soc. Rev. 2006, 35, 1056-1067. (b) Woods, T. J.; Ballesteros-Rivas, M. F.; Ostrovsky, S. M.; Palii, A. V.; Reu, O. S.; Klokishner, S. I.; Dunbar, K. R. Strong Direct Magnetic Coupling in a Dinuclear CoII Tetrazine Radical Single-Molecule Magnet. Chem. - Eur. J. 2015, 21, 10302-10305. (c) Alexandropoulos, D. I.; Dolinar, B. S.; Vignesh, K. R.; Dunbar, K. R. Putting a New Spin on Supramolecular Metallacycles: Co3 Triangle and Co4 Square Bearing Tetrazine-Based Radicals as Bridges. J. Am. Chem. Soc. 2017, 139, 11040-11043. (d) Lemes, M. A.; Brunet, G.; Pialat, A.; Ungur, L.; Korobkov, I.; Murugesu, M. Strong Ferromagnetic Exchange Coupling in a {Ni^{II}₄} Cluster Mediated through an Air-Stable Tetrazine-Based Radical Anion. Chem. Commun. 2017, 53, 8660-8663. (e) Woods, T. J.; Stout, H. D.; Dolinar, B. S.; Vignesh, K. R.; Ballesteros-Rivas, M. F.; Achim, C.; Dunbar, K. R. Strong Ferromagnetic Exchange Coupling Mediated by a Bridging Tetrazine Radical in a Dinuclear Nickel Complex. Inorg. Chem. 2017, 56, 12094-12097. (f) Lemes, M. A.; Stein, H. N.; Gabidullin, B.; Robeyns, K.; Clérac, R.; Murugesu, M. Probing Magnetic-Exchange Coupling in Supramolecular Squares Based on Reducible Tetrazine-Derived Ligands. Chem. - Eur. J. 2018, 24, 4259-4263.
- (9) Gatteschi, D.; Sessoli, R.; Villain, J. Molecular Nanomagnets; Oxford University Press: 2006.
- (10) Guo, Z.; Deng, Y.-F.; Zhang, Y.; Pikramenou, Z.; Zhang, Y.-Z. Two Azido-Bridged [2 × 2] Cobalt(II) Grids Featuring Single-Molecule Magnet Behaviour. *Dalton Trans.* **2020**, *49*, 9218–9222.
- (11) Patra, S.; Sarkar, B.; Ghumaan, S.; Fiedler, J.; Kaim, W.; Lahiri, G. K. Isovalent and Mixed-Valent Diruthenium Complexes [(acac)₂Ru^{II} (μ-bpytz)Ru^{II}(acac)₂] and [(acac)₂Ru^{II}(μ-bpytz)-

- Ru^{III}(acac)₂](ClO₄) (acac = Acetylacetonate and bpytz = 3,6-Bis(3,5-dimethylpyrazolyl)-1,2,4,5-tetrazine): Synthesis, Spectroelectrochemical, and EPR Investigation. *Inorg. Chem.* **2004**, *43*, 6108–6113
- (12) (a) Audebert, P.; Sadki, S.; Miomandre, F.; Clavier, G.; Claude Vernières, M.; Saoud, M.; Hapiot, P. Synthesis of new substituted tetrazines: electrochemical and spectroscopic properties. *New J. Chem.* **2004**, 28, 387–392. (b) Plugge, M.; Alain-Rizzo, V.; Audebert, P.; Brouwer, A. M. Excited state dynamics of 3,6-diaryl-1,2,4,5-tetrazines. Experimental and theoretical studies. *J. Photochem. Photobiol., A* **2012**, 234, 12–20.
- (13) (a) Heath, G. A.; Yellowlees, L. J.; Braterman, P. S. Spectroelectrochemical studies on tris-bipyridyl ruthenium complexes; ultraviolet, visible, and near-infrared spectra of the series [Ru(bipyridyl)-3]2+/1+/0/1-. J. Chem. Soc., Chem. Commun. 1981, 287–289. (b) Braterman, P. S.; Song, J. I.; Peacock, R. D. Electronic absorption spectra of the iron(II) complexes of 2,2'-bipyridine, 2,2'-bipyrimidine, 1,10-phenanthroline, and 2,2':6',2"-terpyridine and their reduction products. Inorg. Chem. 1992, 31, 555–559.
- (14) Murrie, M. Cobalt(ii) single-molecule magnets. Chem. Soc. Rev. 2010, 39, 1986–1995.
- (15) Chilton, N. F.; Anderson, R. P.; Turner, L. D.; Soncini, A.; Murray, K. S. PHI: A Powerful New Program For the Analysis of Anisotropic Monomeric and Exchange-Coupled Polynuclear d- and f-Block Complexes. *J. Comput. Chem.* **2013**, *34*, 1164–1175.
- (16) Scalapino, D. J.; Imry, Y.; Pincus, P. Generalized Ginzburg-Landau theory of pseudo-one-dimensional systems. *Phys. Rev. B* **1975**, *11*, 2042–2048.
- (17) (a) Saber, M. R.; Dunbar, K. R. Ligands effects on the magnetic anisotropy of tetrahedral cobalt complexes. *Chem. Commun.* **2014**, *50*, 12266–12269. (b) Zhang, Y.-Z.; Gómez-Coca, S.; Brown, A. J.; Saber, M. R.; Zhang, X.; Dunbar, K. R. Trigonal antiprismatic Co(II) single molecule magnets with large uniaxial anisotropies: importance of Raman and tunneling mechanisms. *Chem. Sci.* **2016**, *7*, 6519–6527.
- (18) Mydosh, J. Spin Glasses: An Experimental Introduction; CRC Press: London, 1993.
- (19) Carlin, R. L. Magnetochemistry; Springer-Verlag: Berlin, 1986.
- (20) (a) Milios, C. J.; Vinslava, A.; Wernsdorfer, W.; Moggach, S.; Parsons, S.; Perlepes, S. P.; Christou, G.; Brechin, E. K. A Record Anisotropy Barrier for a Single-Molecule Magnet. *J. Am. Chem. Soc.* **2007**, *129*, 2754–2755. (b) Chakarawet, K.; Bunting, P. C.; Long, J. R. Large Anisotropy Barrier in a Tetranuclear Single-Molecule Magnet Featuring Low-Coordinate Cobalt Centers. *J. Am. Chem. Soc.* **2018**, *140*, 2058–2061.
- (21) (a) Miyasaka, H.; Takayama, K.; Saitoh, A.; Furukawa, S.; Yamashita, M.; Clérac, R. Three-Dimensional Antiferromagnetic Order of Single-Chain Magnets: A New Approach to Design Molecule-Based Magnets. *Chem. Eur. J.* 2010, 16, 3656–3662. (b) Zhang, Y.-Z.; Zhao, H.-H.; Funck, E.; Dunbar, K. R. A Single-Chain Magnet Tape Based on Hexacyanomanganate(III). *Angew. Chem., Int. Ed.* 2015, 54, 5583–5587.
- (22) Dhers, S.; Feltham, H. L. C.; Brooker, S. A toolbox of building blocks, linkers and crystallisation methods used to generate single-chain magnets. *Coord. Chem. Rev.* **2015**, 296, 24–44.